Applied Numerical Mathematics 95 (2015) 280–291

Contents lists available at ScienceDirect

Applied Numerical Mathematics

www.elsevier.com/locate/apnum

# Numerical solution of a multidimensional sedimentation problem using finite volume-element methods

Ricardo Ruiz-Baier [a,*], Héctor Torres [b]

[a] ISTE-FGSE, University of Lausanne, Géopolis UNIL-Mouline, CH-1015 Lausanne, Switzerland
[b] Departamento de Matemáticas, Facultad de Ciencias, Universidad de La Serena, Av. Cisternas 1200, La Serena, Chile

ARTICLE INFO

*Article history:*
Available online 17 March 2014

*Keywords:*
Finite volume element method
Sedimentation–consolidation process
Navier–Stokes equations
Inclined channels

ABSTRACT

We are interested in the reliable simulation of the sedimentation of monodisperse suspensions under the influence of body forces. At the macroscopic level, the complex interaction between the immiscible fluid and the sedimentation of a compressible phase may be governed by the Navier–Stokes equations coupled to a nonlinear advection–diffusion–reaction equation for the local solids concentration. A versatile and effective finite volume element (FVE) scheme is proposed, whose formulation relies on a stabilized finite element (FE) method with continuous piecewise linear approximation for velocity, pressure and concentration. Some numerical simulations in two and three spatial dimensions illustrate the features of the present FVE method, suggesting their applicability in a wide range of problems.



## 1. Introduction

Gravitational sedimentation of small particles dispersed in a viscous fluid is a phenomenon widely observed in many engineering applications and natural systems. Such a process, where gravity drives the separation of the suspension into a clear supernatant liquid and a consolidated sediment, is typically employed in e.g. the solid–liquid separation of suspensions in mineral processing and wastewater treatment. Historically, many sedimentation models were based on the one-dimensional sedimentation theory by Kynch [26], which basically consists in describing the solids concentration as a function of vessel depth and time, governed by a scalar, nonlinear hyperbolic conservation law. This prototype model, along with a large number of tailored variants, have been proven to be accurate enough to represent some specific industrial scenarios such as clarifying–thickening processes and mixture of polydisperse suspensions (see e.g. [15,17]). Here we are more interested in multidimensional models that are able to predict some additional effects, such as the direct influence of bulk flow and boundary conditions. This necessarily entails the solution of the Navier–Stokes equations for the flow field of the mixture, increasing the complexity of the mathematical description of a strongly coupled system and also making difficult to solve these equations numerically. We focus our study in the particular case of batch sedimentation in closed channels exhibiting different geometries. The phenomenon of enhanced gravity settling in inclined channels, known as the Boycott effect, was first reported in [9] in the context of erythrocyte sedimentation. In such a context, the process of settling is enhanced when the vessel is tilted from the gravity force direction. A theoretical study of this phenomenon was later developed in

* Corresponding author. Tel.: +41 21 692 44 09.
*E-mail addresses:* ricardo.ruizbaier@unil.ch (R. Ruiz-Baier), htorres@userena.cl (H. Torres).

http://dx.doi.org/10.1016/j.apnum.2013.12.006
0168-9274/

the framework of fluid mechanics [24]. Since many years, the performance of inclined settlers has been described using the Ponder–Nakamura–Kuroda theory (see [36,35,21]), which does not consider the kinetics of the fluid motion. In [1] the authors generalized this theory by including a continuity equation for each phase, solid and fluid, an equation to describe the movement of the suspension as a continuum, and constitutive relationships between the velocities of each phase. In this context, our goal is to describe at least some components in the overall performance of inclined settlers such as the behavior of the layer of clear fluid along the underside of the inclined wall, which is accelerated upwards, and that enhances the sedimentation process. Even if multidimensional models of batch sedimentation show that the assumed one-dimensional nature of the concentration profile holds true in many scenarios, this is not the case for the velocity. Depending on the flow regime, it can drive the dynamics of the solids concentration and a number of variations in the flow field can be observed.

Besides experimental and theoretical investigations on the physics of sedimentation processes, numerical simulation is still an important tool to study the behavior of these phenomena. It provides an inexpensive way to try different configurations, nonstandard settings and special conditions for a given process. An important amount of work has been devoted to the determination of exact and numerical solution of related equations (see e.g. [8] and the references therein). Most of these contributions focus in the one-dimensional case, where all flow variables are assumed horizontally invariant and, subsequently, flow properties and boundary conditions can be replaced by modifications to the flux function, implying that only the concentration equation needs to be solved. More general models and solvers in two or three spatial dimensions include e.g. [31,32,27,13], where numerical studies of batch sedimentation in rectangular channels have been presented. Due to the nonlinearity and degeneracy of the concentration equation, traditional approaches are often unreliable and nonstandard techniques such as mixed or hybrid methods are needed. These difficulties also arise in e.g. the modelling of multiphase flows in porous media (see [4,29,40,37] and the references therein for the implementation and analysis of mixed finite elements/finite volumes of closely related equations).

Continuity equations can be solved numerically by a large variety of methods, each of them featuring some desirable properties. For instance, classical finite differences and finite volumes in structured meshes are straightforward to implement and can allow for conservative approximations, whereas finite element methods are robust and permit natural derivation of error estimates provided that the solution has enough regularity. Many modifications and combinations of these classical methods have been proposed to solve flow problems. Here we focus on one of these hybrid strategies, the finite volume element (FVE) method, that goes back to the early works [18,6]. Several variants of the FVE method are available from the literature, but irrespective of the specific form at hand, the main idea is that local conservativity is inherited from the finite volume part of the method, while maintaining the versatility and systematic error analysis in the $L^2$-norm. The FVE introduced in this paper is a special class of Petrov–Galerkin methods where the trial function spaces are connected with the test function spaces associated with the dual partition induced by the control volumes [38,28]. In summary, the method is able to effectively treat arbitrarily complex geometries and unstructured meshes, a variety of boundary conditions, and features local conservation and front capturing properties.

Works closely related to the present paper include the FVE method applied to Boussinesq equations analyzed in [30], the hybrid FE–FV scheme for incompressible flows presented in [19] and the ones for shear dependent viscoelastic flows from [34,46], the FV multiresolution method proposed in [13], and the stabilized FVE formulation for sedimentation problems in axisymmetric domains introduced in [14]. Our contribution represents an extension to the formers in that we consider flocculated suspensions (which translates in adding a degenerate diffusive term to the concentration equation), and to the latter in the sense that we cover the full three-dimensional case, and employ the Navier–Stokes equations for describing the flow. In addition, we use only one dual mesh, an interior penalty stabilization, and our formulation is based on piecewise continuous finite elements for all fields. The convergence analysis of (a regularized version of) the problem will be postponed for a future contribution.

The remainder of this paper is organized as follows. In Section 2 we recall some basic notation and state the model problem, specifying the conservation equations, constitutive relations, and weak formulation. The fully discrete FVE formulation is derived in Section 3, and Section 4 contains several numerical results illustrating the physical behavior of the system and the accuracy and robustness of the proposed FVE method. Concluding remarks and perspectives are collected in Section 5.

## 2. Preliminaries and statement of the initial–boundary value problem

We will consider the usual notation for Sobolev spaces $W^{m,k}(\Omega)$. The norm of $H^k(\Omega) = W^{k,2}(\Omega)$ is denoted by $\|\cdot\|_{k,\Omega}$ and the subscript $\Omega$ will be omitted unless otherwise specified.

The governing equations for the sedimentation–consolidation process in an immiscible fluid can be written as follows (see e.g. [11,15,22]):

$$\partial_t \phi + \operatorname{div} \boldsymbol{f}(\phi, \boldsymbol{u}) = \Delta A(\phi), \tag{2.1a}$$

$$\partial_t \boldsymbol{u} + \boldsymbol{u} \cdot \nabla \boldsymbol{u} - \mathbf{div}\big(\mu(\phi)\boldsymbol{\varepsilon}(\boldsymbol{u}) - \lambda p \mathbf{I}\big) = \boldsymbol{g}(\phi), \tag{2.1b}$$

$$\lambda \operatorname{div} \boldsymbol{u} = 0, \quad \text{in } \Omega, \quad t > 0. \tag{2.1c}$$

The problem is defined for a given Lipschitz continuous domain $\Omega \subset \mathbb{R}^d$ $(d = 2, 3)$ with polyhedral boundary $\partial\Omega$ and outward pointing normal $\boldsymbol{n}$. The unknowns are the local solids concentration $\phi$, the local volume-average velocity of the

mixture $\boldsymbol{u}$, and the pressure $p$. Moreover, $\boldsymbol{f}$ is a flux vector which is linear in $\boldsymbol{u}$ but nonlinear in $\phi$, $A$ is a nonlinear, non-decreasing diffusion function modelling sediment compressibility, $\mu(\phi)\boldsymbol{\varepsilon}(\boldsymbol{u}) - \lambda p\mathbf{I}$ is the Cauchy stress tensor, where $\boldsymbol{\varepsilon}(\boldsymbol{u}) := \frac{1}{2}(\nabla\boldsymbol{u} + \nabla\boldsymbol{u}^{\mathrm{T}})$ is the strain rate tensor, $\mu$ is the concentration-dependent viscosity of the fluid, $\lambda$ is a positive parameter, and $\boldsymbol{g}$ is a forcing term describing the local density fluctuations.

The model is complemented by initial data for the concentration $\phi$ and the velocity $\boldsymbol{u}$, and boundary conditions as follows. The velocity field is fixed $\boldsymbol{u} = \boldsymbol{u}_{\mathrm{D}} \in L^2(\Gamma)$ on $\Gamma = \partial\Omega$. In particular, the vessel is continuously fed through the inflow boundary $\Gamma_{\mathrm{in}}$ with feed suspension, which corresponds to a given profile for the velocity $\boldsymbol{u}_{\mathrm{in}}$, and a feed concentration $\phi_{\mathrm{in}}$. On $\Gamma_{\mathrm{out}}$ we prescribe a volume underflow velocity $\boldsymbol{u}_{\mathrm{out}}$ at which the thickened sediment is removed from the unit and zero-flux conditions are assumed for $\phi$. On the remaining part of $\partial\Omega$ we specify no-slip boundary data for the velocity field ($\boldsymbol{u} = \mathbf{0}$), and zero-flux boundary conditions for the concentration.

The flux vector in (2.1a) is given by $\boldsymbol{f}(\phi, \boldsymbol{u}) = \phi\boldsymbol{u} + f_{\mathrm{bk}}(\phi)\boldsymbol{k}$, where $\boldsymbol{k}$ is the unit vector pointing in the direction of gravity and $f_{\mathrm{bk}}$ is the Kynch batch flux density function [26] describing hindered settling. This function is assumed to satisfy $f_{\mathrm{bk}}(0) = f_{\mathrm{bk}}(\phi_{\max}) = 0$ and $f_{\mathrm{bk}}(\phi) > 0$ for $0 < \phi < \phi_{\max}$, where $0 < \phi_{\max} \leqslant 1$ is a maximum concentration [11]. Specifically, we choose [33]

$$f_{\mathrm{bk}}(\phi) = \begin{cases} u_\infty \phi(1 - \phi/\phi_{\max})^{n_{\mathrm{MB}}} & \text{for } 0 < \phi < \phi_{\max}, \\ 0 & \text{otherwise,} \end{cases} \qquad n_{\mathrm{MB}} \geqslant 1,$$

where $u_\infty > 0$ is the settling velocity of a single particle in an unbounded fluid, and we choose the exponent $n_{\mathrm{MB}} = 2$.

The term $\Delta A(\phi)$ models sediment compressibility, where the integrated diffusion function $A$ is given by

$$A(\phi) = \int_0^\phi a(s)\,\mathrm{d}s, \quad \text{where } a(\phi) := \frac{f_{\mathrm{bk}}(\phi)\sigma_{\mathrm{e}}'(\phi)}{(\varrho_{\mathrm{s}} - \varrho_{\mathrm{f}})g\phi}.$$

Here $\varrho_{\mathrm{s}}$ and $\varrho_{\mathrm{f}}$ are the solid and fluid mass densities, respectively, $g$ is the acceleration of gravity, and $\sigma_{\mathrm{e}}'$ is the derivative of effective solid stress function, assumed to satisfy $\sigma_{\mathrm{e}}'(0) = 0$, $\sigma_{\mathrm{e}}'(\phi) > 0$ for $\phi > 0$. Since $a(0) = a(\phi_{\max}) = 0$ and $a(\phi) > 0$ for $0 < \phi < \phi_{\max}$, (2.1a) is a two-point degenerate parabolic PDE, which degenerates into a first-order hyperbolic conservation law for $\phi = 0$ and $\phi = \phi_{\max}$.

The forcing term $\boldsymbol{g}(\phi) = C\phi\lambda\boldsymbol{k}$ in (2.1b) models that the mixture flow is also driven by local fluctuations of $\phi$. Finally, $\mu(\phi)$ denotes a generalized local concentration-dependent Newtonian viscosity function, where we assume that there exist constants $\mu_{\min}, \mu_{\max} > 0$ such that $\mu_{\min} < \mu(s) < \mu_{\max}$ for $s \in \mathbb{R}_+$. A suitable choice is $\mu(\phi) = (1 - \phi/\tilde{\phi}_{\max})^{-\beta}$, where $\tilde{\phi}_{\max}$ is a nominal maximum concentration, chosen such that $\tilde{\phi}_{\max} > \phi_{\max}$.

After introduction of the functional spaces $\boldsymbol{\mathcal{V}} = \{\boldsymbol{v} \in \boldsymbol{H}^1(\Omega)\colon\ \boldsymbol{v} = \boldsymbol{v}_{\mathrm{D}} \text{ on } \Gamma\}$, $Q = L^2_0(\Omega)$, and $S := H^1(\Omega)$, the variational formulation for (2.1) reads: Find $\phi \in H^1(0,T;S)$, $\boldsymbol{u} \in \mathbf{H}^1(0,T;\boldsymbol{\mathcal{V}})$, $p \in L^2(0,T;Q)$ such that

$$\begin{aligned}
&(\phi_t, \psi)_\Omega + (\boldsymbol{u}\cdot\nabla\phi, \psi)_\Omega - \big(f_{\mathrm{bk}}(\phi)\boldsymbol{k}, \nabla\psi\big)_\Omega - \big(\nabla A(\phi), \nabla\psi\big)_\Omega = 0 \quad \forall\psi \in S,\\
&(\boldsymbol{u}_t, \boldsymbol{v})_\Omega + \big((\boldsymbol{u}\cdot\nabla)\boldsymbol{u}, \boldsymbol{v}\big)_\Omega + \big(\mu(\phi)\boldsymbol{\varepsilon}(\boldsymbol{u}), \boldsymbol{\varepsilon}(\boldsymbol{v})\big)_\Omega - \lambda(p, \operatorname{div}\boldsymbol{v})_\Omega - \big(\boldsymbol{g}(\phi), \boldsymbol{v}\big)_\Omega = 0 \quad \forall\boldsymbol{v} \in \boldsymbol{\mathcal{V}},\\
&\lambda(q, \operatorname{div}\boldsymbol{u})_\Omega = 0 \quad \forall q \in Q,
\end{aligned} \tag{2.2}$$

where $(\cdot,\cdot)_\Omega$ denotes the inner product in $L^2(\Omega)$. Existence of weak solutions to (2.2) can be proved after adequate parabolic regularization of the degenerate diffusion term of the concentration equation, and under some additional assumptions, such as large enough fluid viscosity (see e.g. [12, Lemma 3]).

## 3. Approximation by finite volume elements

Throughout the text, $\mathcal{T}_h$ denotes a primal mesh of closed triangular (or tetrahedral, for $d = 3$) elements $K$ of diameter $h_K$, which is assumed to be locally regular, that is, there exists $C > 0$ such that

$$\frac{h_K}{\varrho_K} \leqslant C, \quad \text{for all } K \in \mathcal{T}_h,$$

where $\varrho_K$ denotes the diameter of the largest ball contained in $K$. The mesh parameter is $h = \max_{K\in\mathcal{T}_h}\{h_K\}$.

A dual mesh $\mathcal{T}_h^\star$ is created by connecting the center of gravity $b_K$ of an element $K \in \mathcal{T}_h$ with the midpoints (2D barycenters) of each face $F \subset \partial K$, forming four polyhedra $K_z$ for $z$ in the set of vertexes of $K$ (see Fig. 1). Let $S = \{s_j,\ j = 1,\ldots,N_h\}$ be the set of nodes of $\mathcal{T}_h$. To each vertex $s_j$ we associate a so-called control volume $K_j^\star$ consisting of the union of the polyhedra $K_{s_j}$ sharing the vertex $s_j$.

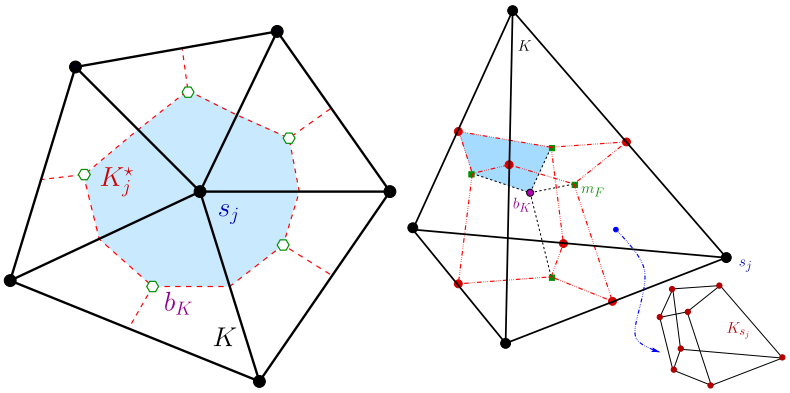


**Fig. 1.** Sketch of elements in the primal mesh $\mathcal{T}_h$ (in solid lines) and interior node-centered control volumes of the dual mesh $\mathcal{T}_h^\star$ (in dashed lines) on a local 2D patch (left) and a single primal tetrahedron split into four polyhedra (right).

Let us introduce the following finite dimensional spaces associated with the primal and dual partitions

$$\boldsymbol{\mathcal{V}}_h := \big\{\boldsymbol{v} \in \boldsymbol{H}^1(\Omega) \cap \boldsymbol{C}^0(\overline{\Omega})\colon\ \boldsymbol{v}|_K \in \mathbb{P}_1(K)^d \text{ for all } K \in \mathcal{T}_h,\ \boldsymbol{v}|_F = \boldsymbol{u}_{\mathrm{D}},\ \text{if } F \subset \partial K \text{ lies on } \partial\Omega\big\},$$

$$Q_h := \big\{q \in L^2_0(\Omega) \cap C^0(\overline{\Omega})\colon\ q|_K \in \mathbb{P}_1(K) \text{ for all } K \in \mathcal{T}_h\big\},$$

$$S_h := \big\{s \in H^1(\Omega)\colon\ s|_K \in \mathbb{P}_1(K) \text{ for all } K \in \mathcal{T}_h\big\},$$

$$\boldsymbol{\mathcal{V}}_h^\star := \big\{\boldsymbol{v} \in \mathbf{L}^2(\Omega)\colon\ \boldsymbol{v}|_{K_j^\star} \in \mathbb{P}_0\big(K_j^\star\big)^d \text{ for all } K_j^\star \in \mathcal{T}_h^\star,\ \boldsymbol{v}|_{K_j^\star} = \boldsymbol{u}_{\mathrm{D}} \text{ if } K_j^\star \text{ is a boundary volume}\big\},$$

$$S_h^\star := \big\{s \in L^2(\Omega)\colon\ s|_{K_j^\star} \in \mathbb{P}_0\big(K_j^\star\big) \text{ for all } K_j^\star \in \mathcal{T}_h^\star\big\},$$

where $\mathbb{P}_m(K)$ denotes the space of polynomial functions of total degree $s \leqslant m$ defined on the element $K$. Notice that Dirichlet data are imposed for $\boldsymbol{u}$ in the definition of $\boldsymbol{\mathcal{V}}_h$ and $\boldsymbol{\mathcal{V}}_h^\star$. In addition, we define the $\mathcal{T}_h^\star$-piecewise lumping maps $\mathcal{P}_h : \boldsymbol{\mathcal{V}}_h \to \boldsymbol{\mathcal{V}}_h^\star$ and $\mathcal{Q}_h : S_h \to S_h^\star$ relating the primal and dual meshes (cf. [38]) by

$$\boldsymbol{v}_h(x) = \sum_{j=1}^{N_h} \boldsymbol{v}_h(s_j)\boldsymbol{\varphi}_j(x) \mapsto \mathcal{P}_h\boldsymbol{v}_h(x) = \sum_{j=1}^{N_h} \boldsymbol{v}_h(s_j)\boldsymbol{\chi}_j(x),$$

$$\mathcal{Q}_h\psi_h(x) = \sum_{j=1}^{N_h} \psi_h(s_j)\chi_j(x), \quad x \in \Omega,$$

for all $\boldsymbol{v}_h \in \boldsymbol{\mathcal{V}}_h$, $\psi_h \in S_h$ where $\chi_j$ and $\boldsymbol{\chi}_j$ are the scalar and vectorial characteristic functions of the control volume $K_j^\star$ and $\{\boldsymbol{\varphi}_i\}_i$ is the canonical FE basis of $\boldsymbol{\mathcal{V}}_h$. For any $(\boldsymbol{w}, \psi) \in \boldsymbol{H}^1(\Omega) \times H^1(\Omega)$ these operators satisfy the following interpolation properties

$$\|\boldsymbol{w} - \mathcal{P}_h\boldsymbol{w}\|_0 \leqslant Ch|\boldsymbol{w}|_1, \qquad \|\psi - \mathcal{Q}_h\psi\|_0 \leqslant Ch|\psi|_1.$$

The discrete problem associated with the variational formulation (2.2) is obtained by multiplying (2.1a) by $\psi_h^\star \in S_h^\star$, integrating by parts over each control volume $K_i^\star \in \mathcal{T}_h^\star$, multiplying (2.1b) by $\boldsymbol{v}_h^\star \in \boldsymbol{\mathcal{V}}_h^\star$ and integrating by parts over each $K_i^\star \in \mathcal{T}_h^\star$, and multiplying (2.1c) by $q_h \in Q_h$ and integrating by parts over each element $K \in \mathcal{T}_h$. This, along with the definition of $\boldsymbol{f}$, gives the Petrov–Galerkin formulation: For $0 < t \leqslant T$, find $\phi_h(t) \in S_h$, $\boldsymbol{u}_h(t) \in \boldsymbol{\mathcal{V}}_h$, $p_h(t) \in Q_h$ such that

$$\frac{\mathrm{d}}{\mathrm{d}t}\big(\phi_h(t), \psi_h^\star\big)_\Omega + \sum_{i=1}^{N_h} \int_{\partial K_i^\star} \big(\boldsymbol{u}_h(t) \cdot \boldsymbol{n}_{K_i^\star}\big)\phi_h(t)\psi_h^\star \,\mathrm{d}\sigma$$

$$- \sum_{i=1}^{N_h} \int_{\partial K_i^\star} f_{\mathrm{bk}}\big(\phi_h(t)\big)(\boldsymbol{n}_{K_i^\star} \cdot \boldsymbol{k})\psi_h^\star(s_i)\,\mathrm{d}\sigma - \sum_{i=1}^{N_h} \int_{\partial K_i^\star} \partial_{\boldsymbol{n}} A\big(\phi_h(t)\big)\psi_h^\star(s_i)\,\mathrm{d}\sigma = 0,$$

$$\frac{\mathrm{d}}{\mathrm{d}t}\big(\boldsymbol{u}_h(t),\boldsymbol{v}_h^\star\big)_\Omega+\sum_{i=1}^{N_h}\int_{\partial K_i^\star}\big(\boldsymbol{u}_h(t)\cdot\boldsymbol{n}_{K_i^\star}\big)\big(\boldsymbol{u}_h(t)\cdot\boldsymbol{v}_h^\star(s_i)\big)\,\mathrm{d}\sigma$$

$$-\sum_{i=1}^{N_h}\int_{\partial K_i^\star}\mu\big(\phi_h(t)\big)\boldsymbol{v}_h^\star(s_i)\partial_{\boldsymbol{n}}\boldsymbol{u}_h(t)\,\mathrm{d}\sigma-\lambda\sum_{i=1}^{N_h}\int_{\partial K_i^\star}p_h\boldsymbol{v}_h^\star(s_i)\boldsymbol{n}_{K_i^\star}\,\mathrm{d}\sigma=\big(\boldsymbol{g}\big(\phi_h(t)\big),\boldsymbol{v}_h^\star\big)_\Omega,$$

$$\lambda\sum_{i=1}^{N_h}\boldsymbol{u}_h(s_i,t)\cdot\int_{\partial K_i^\star}q_h\boldsymbol{n}_{K_i^\star}\,\mathrm{d}\sigma=0,$$

for all $\psi_h^\star\in S_h^\star$, $\boldsymbol{v}_h^\star\in\boldsymbol{\mathcal{V}}_h^\star$, $q_h\in Q_h$. Using Lemma 3.1 from [14] and Lemma 3 from [30] we can state the following space semi-discrete FVE method: For $0<t\leqslant T$, find $\phi_h(t)\in S_h$, $\boldsymbol{u}_h(t)\in\boldsymbol{\mathcal{V}}_h$, $p_h(t)\in Q_h$ such that

$$\big(\phi_h'(t),\mathcal{Q}_h\psi_h\big)_\Omega+\big(\boldsymbol{u}_h(t)\cdot\nabla\phi_h(t),\psi_h\big)_\Omega-\big(f_{\mathrm{bk}}(\phi_h)\boldsymbol{k},\nabla\psi_h\big)_\Omega-\big(\nabla A(\phi_h),\nabla\psi_h\big)_\Omega=0,$$

$$\frac{\mathrm{d}}{\mathrm{d}t}\big(\boldsymbol{u}_h(t),\mathcal{P}_h\boldsymbol{v}_h\big)_\Omega+\big(\big(\boldsymbol{u}_h(t)\cdot\nabla\big)\boldsymbol{u}_h(t),\boldsymbol{v}_h\big)_\Omega+\big(\mu\big(\phi_h(t)\big)\boldsymbol{\varepsilon}\big(\boldsymbol{u}_h(t)\big),\boldsymbol{\varepsilon}(\boldsymbol{v}_h)\big)_\Omega$$

$$-\lambda\big(p_h(t),\operatorname{div}\boldsymbol{v}_h\big)_\Omega-\big(\boldsymbol{g}\big(\phi_h(t)\big),\mathcal{P}_h\boldsymbol{v}_h\big)_\Omega=0,$$

$$\lambda\big(q_h,\operatorname{div}\boldsymbol{u}_h(t)\big)_\Omega=0,$$

for all $\psi_h\in S_h$, $\boldsymbol{v}_h\in\boldsymbol{\mathcal{V}}_h^0=\boldsymbol{\mathcal{V}}_h\cap\boldsymbol{H}_0^1(\Omega)$, $q_h\in Q_h$. A uniform partition of the interval $[0,T]$ is done into $N_T$ sub-intervals of size $\Delta t$ and as time integrator we employ a second order backward difference advancing scheme (BDF2, see e.g. [39]). Only the nonlinear diffusion and concentration-driven part of the flux in the concentration equation are treated explicitly. This restriction will have an influence in the overall CFL condition, and for the moment we leave further investigation to a forthcoming study. The remaining nonlinearities (convection and coupling terms) are considered implicit, so that at each time iteration the solution to the system of nonlinear equations is approximated with a fixed point algorithm. The nonlinear fully discrete scheme reads:

$$\frac{1}{\Delta t}\big(\tilde{\phi}_h^{n+1},\psi_h\big)_\Omega+\big(\boldsymbol{u}_h^{n+1}\cdot\nabla\phi_h^{n+1},\psi_h\big)_\Omega-\big({f_{\mathrm{bk}}}^n\boldsymbol{k},\nabla\psi_h\big)_\Omega-\big(\nabla A_h^n,\nabla\psi_h\big)_\Omega=0,$$

$$\frac{1}{\Delta t}\big(\tilde{\boldsymbol{u}}_h^{n+1},\boldsymbol{v}_h\big)_\Omega+\big(\big(\boldsymbol{u}_h^{n+1}\cdot\nabla\big)\boldsymbol{u}_h^{n+1},\boldsymbol{v}_h\big)_\Omega+\big(\mu_h^{n+1}\boldsymbol{\varepsilon}\big(\boldsymbol{u}_h^{n+1}\big),\boldsymbol{\varepsilon}(\boldsymbol{v}_h)\big)_\Omega-\lambda\big(p_h^{n+1},\operatorname{div}\boldsymbol{v}_h\big)_\Omega-\big(\boldsymbol{g}_h^{n+1},\mathcal{P}_h\boldsymbol{v}_h\big)_\Omega=0,$$

$$\lambda\big(q_h,\operatorname{div}\boldsymbol{u}_h^{n+1}\big)_\Omega=0,\tag{3.3}$$

for all $\psi_h\in S_h$, $\boldsymbol{v}_h\in\boldsymbol{\mathcal{V}}_h^0$, $q_h\in Q_h$, where ${f_{\mathrm{bk}}}^n:=f_{\mathrm{bk}}(\phi_h^n)$, $A_h^n:=A(\phi_h^n)$, and $\tilde{s}_h^{n+1}:=\frac{3}{2}s_h^{n+1}-2s_h^n+\frac{1}{2}s_h^{n-1}$, for $s\in\{\boldsymbol{u}_h,\phi_h\}$.

Unless a stabilization strategy is applied, the present form of this method fails to satisfy the discrete inf–sup condition relating $\boldsymbol{\mathcal{V}}_h$ and $Q_h$, and the numerical solution is prone to spurious oscillations. Therefore, and following [16], we proceed to stabilize the formulation by adding to the LHS of the second equation in (3.3) the following (nonlinear, but taken explicit) extra term arising from a variational multiscale (VMS) analysis

$$\sum_{K\in\mathcal{T}_h}\int_K\tau\big(\boldsymbol{u}_h^n\cdot\nabla\big)\boldsymbol{v}_h\cdot\left[\frac{1}{\Delta t}\tilde{\boldsymbol{u}}_h^{n+1}+\boldsymbol{u}_h^n\cdot\nabla\boldsymbol{u}_h^{n+1}+\nabla p_h\right]\mathrm{d}x,$$

where $\tau$ is an adimensional stabilization parameter depending on $h$ and $\|\boldsymbol{u}_h^n\otimes\boldsymbol{u}_h^n\|_0$ (see also [25,7]). We found that this strategy is sufficiently accurate for the cases studied herein.

## 4. Numerical results

In what follows we study the properties of our FVE method in the framework of coupled systems modelling sedimentation problems. We present a set of numerical examples in two and three dimensions, where we first verify the spatial and temporal accuracy of the approximations. A fixed point algorithm with a tolerance of 1e−8 is used for the algebraic

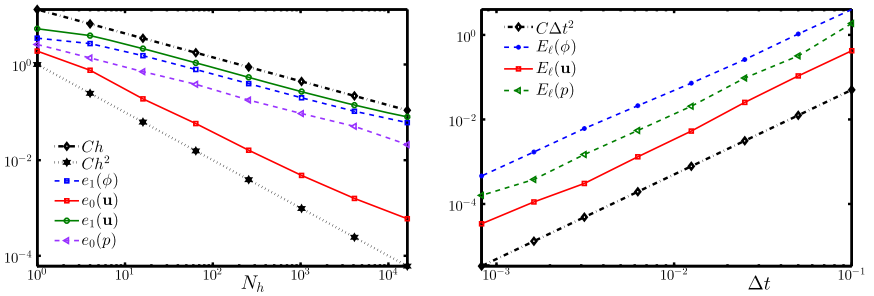


**Fig. 2.** Experimental convergence rates of the FVE scheme applied to (4.4). Spatial convergence in terms of errors (4.5) computed at $T = 1$ with a fixed timestep $\Delta t = 0.001$ (left), and temporal convergence computed in $(0, T)$ with a fixed meshsize $h = 0.0110485$ (right).

system of nonlinear equations and the resulting linear systems are solved with an iterative GMRES method with incomplete LU preconditioning [41].

### 4.1. Accuracy assessment

Our first example addresses the experimental spatial and temporal convergence of the FVE scheme applied to the following coupled problem, where the only nonlinearities are the convection terms: Find $\boldsymbol{u}$, $\phi$, $p$ such that

$$\begin{aligned} &\partial_t \boldsymbol{u} + \boldsymbol{u}\cdot\nabla\boldsymbol{u} - \mathbf{div}\,\boldsymbol{\varepsilon}(\boldsymbol{u}) + \nabla p - e_2\phi = \boldsymbol{f}, \\ &\operatorname{div}\boldsymbol{u} = 0, \\ &\partial_t\phi + \boldsymbol{u}\cdot\nabla\phi - \Delta\phi = g. \end{aligned} \tag{4.4}$$

The domain under consideration is the square $\Omega = (-1, 1)^2$ and forcing terms, along with initial and Dirichlet boundary conditions for $\boldsymbol{u}$ and $\phi$, are imposed according to the following analytic solutions (see e.g. [5])

$$\boldsymbol{u} = \begin{pmatrix} -\cos(\pi x)\sin(\pi y)\sin(2t) \\ \sin(\pi x)\cos(\pi y)\sin(2t) \end{pmatrix}, \qquad p = -\frac{1}{4}\big(\cos(2\pi x) + \cos(2\pi y)\big)\sin^2(2t),$$

$$\phi = \cos(\pi x)\cos(\pi y)\sin(2t).$$

We assess spatial convergence by computing errors at $T = 1$ on a sequence of nested structured primal meshes, employing a fixed time step $\Delta t = 0.001$. Temporal convergence is studied with a sequence of discretizations of $(0, T)$ with decreasing time steps, employing a fixed meshsize $h = 0.0110485$. Errors in different norms are defined as

$$\begin{aligned} &e_0(\boldsymbol{v}) = \big\|\boldsymbol{v}\big(t^{N_T}\big) - \boldsymbol{v}_h\big(t^{N_T}\big)\big\|_{0,\Omega}, \qquad e_1(\boldsymbol{v}) = \big|\boldsymbol{v}\big(t^{N_T}\big) - \boldsymbol{v}_h\big(t^{N_T}\big)\big|_{1,\Omega}, \\ &e_0(q) = \big\|q\big(t^{N_T}\big) - q_h\big(t^{N_T}\big)\big\|_{0,\Omega}, \qquad e_1(\psi) = \big|\psi\big(t^{N_T}\big) - \psi_h\big(t^{N_T}\big)\big|_{1,\Omega}, \\ &E_\ell(\boldsymbol{v}) = \sum_{n=0}^{N_T}\big\|\boldsymbol{v}\big(t^n\big) - \boldsymbol{v}_h\big(t^n\big)\big\|_{0,\Omega}, \qquad E_\ell(\psi) = \sum_{n=0}^{N_T}\big\|\psi\big(t^n\big) - \psi_h\big(t^n\big)\big\|_{0,\Omega}. \end{aligned} \tag{4.5}$$

These quantities are depicted in Fig. 2, where we observe a spatial convergence of order $h^2$ for the $L^2$-norm of $\boldsymbol{u}$, and of order $h$ for the other fields in their respective norms, whereas a convergence of order $(\Delta t)^2$ is experienced for all variables in the $L^\infty(0, t; L^2(\Omega))$-norm. The latter can be expected for non-degenerate cases (natural convection and related flow problems, see e.g. [23,44]). Under degenerate diffusion, rigorous estimates are not yet available, except only for some particular situations [45].

### 4.2. Numerical validation: Differentially heated tall cavity

System (4.4) corresponds to the Boussinesq equations modelling thermal convection processes. Therefore we may also address the capability of the FVE formulation in recovering some features of the transient flow in a differentially heated cavity. In this context $\phi$ represents the adimensional temperature field. We focus on a domain of aspect ratio 8:1 (see e.g. [20] and the references therein). We set $g = 0$, $\boldsymbol{f} = \boldsymbol{0}$, $\Delta t = 0.01$ and $\delta = \sqrt{\mathrm{Pr}/\mathrm{Ra}}$, $\gamma = (\mathrm{RaPr})^{1/2}$, where $\mathrm{Ra} = 3.4\mathrm{e}5$ and $\mathrm{Pr} = 0.71$ are the Rayleigh and Prandtl numbers, respectively. We compare our results with benchmark tests reported in e.g. [2,20], regarding for instance, temperature profiles at centerlines and velocity–pressure patterns, and a reasonable

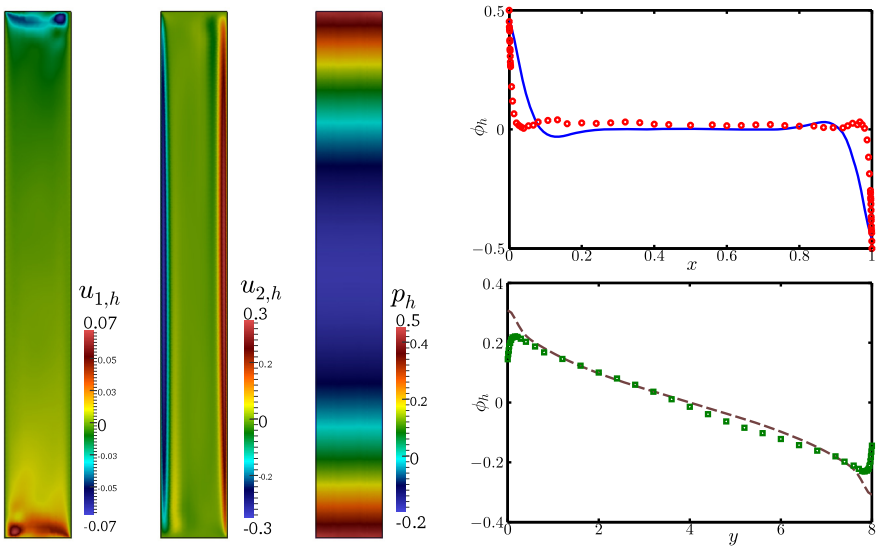


**Fig. 3.** Differentially heated cavity: FVE approximation of velocities and pressure at $t = T$ (left panels), and comparison of obtained temperature profiles at $y = 4$ (right top) and at $x = 0.5$ (right bottom), to benchmark results (circle and square markers).

qualitative agreement is observed (see Fig. 3). Next, we increase the Rayleigh number by about three orders of magnitude and compare the behavior of the temperature distribution on four snapshots of the interval $(0, T)$, with $T = 38$ (Fig. 4). Again, the FVE method is able to capture the main features of the temperature in both regimes (see also [10]).

### 4.3. Boycott effect in an inclined channel

We focus now on the sedimentation of particles described by (2.1), describing in particular the so-called Boycott effect, where the sedimentation of solid particles from solid–liquid suspension is accelerated mainly because the production rate of clarified fluid is higher than that of fluid in vertically oriented vessels. This phenomenon is exploited in several industrial applications. For all remaining cases the diffusion function $A$ vanishes for $\phi \leqslant \phi_c$ provided that the derivative of the effective solid stress function satisfies

$$\sigma_e'(\phi) = \begin{cases} 0 & \text{for } \phi \leqslant \phi_c, \\ \sigma_0 \frac{\alpha}{\phi_c} \left(\frac{\phi}{\phi_c}\right)^{\alpha-1} & \text{otherwise.} \end{cases}$$

We consider an inclined rectangle of height 10 m and width 2 m forming an angle of $\phi$ with the $x$-axis, which we partition into a primal mesh of 7052 triangular elements and 3527 vertexes (see Fig. 5, left). The following physical parameters are employed: $\alpha = 5$, $\eta = 2$, $\beta = 2.5$, $\theta = \pi/3$, $\pi/4$, $\pi/6$, $\lambda = 9000$, $u_\infty = 2.2\text{e}{-3}$, $\phi_c = 0.07$, $\phi_{\max} = 0.95$, $\sigma_0 = 5.5\text{e}{-2}$, $\Delta\rho = 1562$, $C = 0.01$, $g = 9.8$. The mixture is assumed to be initially homogeneous (i.e. $\phi_h(0) = 0.2$) and at rest ($\boldsymbol{u}_h(0) = \mathbf{0}$). We use a timestep of $\Delta t = 0.005$ s, and we simulate the sedimentation process until $t = 500$ s. Numerical solutions for this case are reported in Fig. 6, where independently of the inclination angle, a main vortex is observed at the center of the channel, whereas the material accumulates at the bottom of the domain and a zone of clear fluid starts to form at the top.

### 4.4. Settling in a vessel with inclined walls

A different sedimentation experiment is performed beneath a vessel with downward-facing inclined walls (we refer to [43] for details on the experimental setting). The computational domain is an isosceles trapezoid of height 4.63 m, base of 3.4 m and basal angles of 70°. The primal mesh consists of 10 904 elements and 5453 nodes. We employ the same parameters as in the previous section, except for $\lambda = 100$. This configuration is also motivated by the Boycott effect and an acceleration of the settling is expected. We are interested in observing perturbed horizontal profiles in the concentration field [42], along with relatively high tangential velocities near the boundary layer. The mixture was initially of constant concentration $\phi_h(0) = 0.2$ (or alternatively $\phi_h(0) = 0.08$) and at rest in the whole vessel. Fig. 7 depicts the state of the process at $t = 100$ s, where we confirm the presence of all expected phenomena. In particular we see a more rapid deposition of the material for clearer mixtures. A timestep of $\Delta t = 0.001$ s has been used.

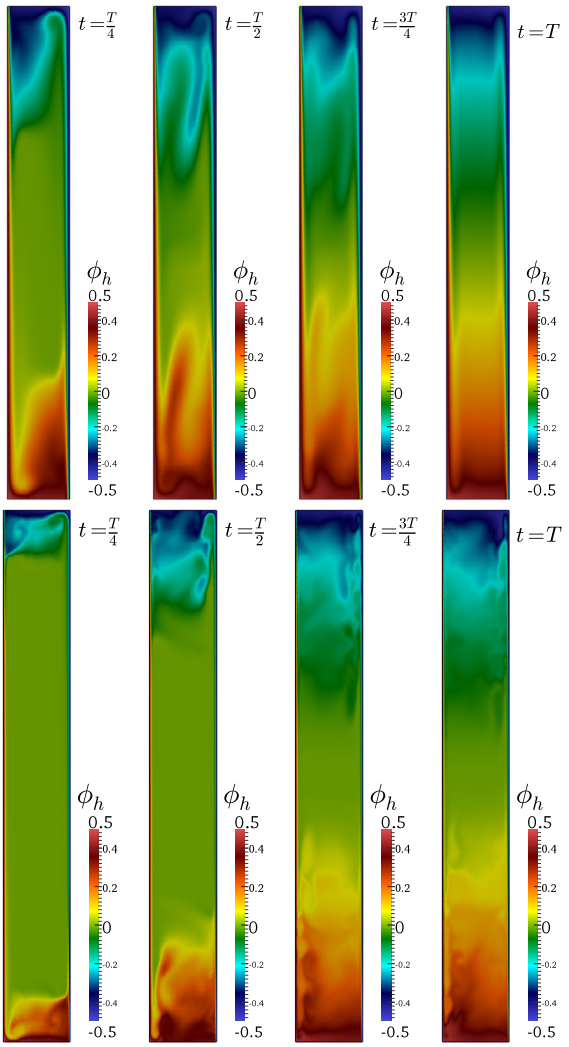


**Fig. 4.** Differentially heated cavity: FVE approximation of temperature at four different times for Ra = 3.4e5 (top panels) and Ra = 3.0e7 (bottom panels).

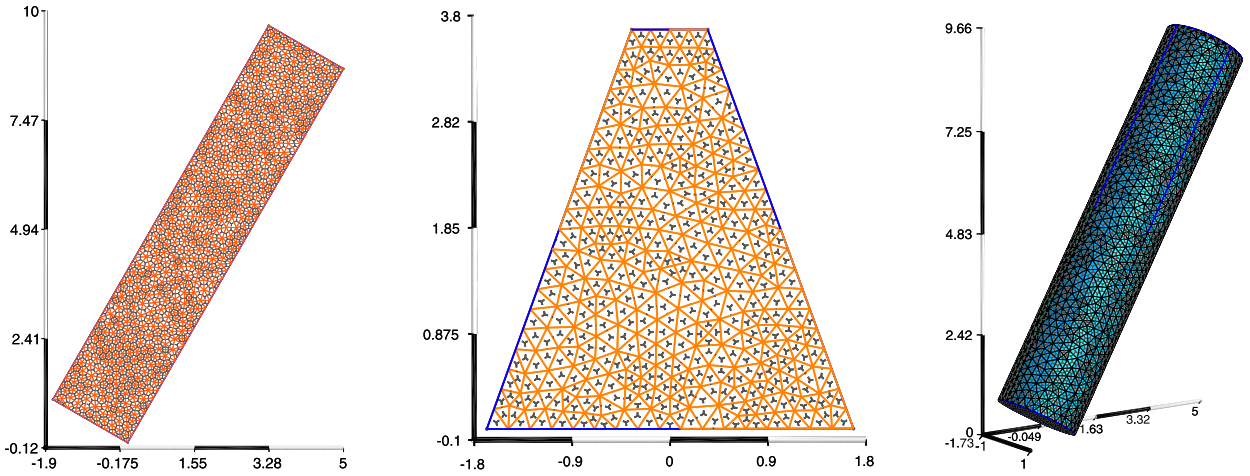


**Fig. 5.** Sketches of primal and dual meshes employed in Sections 4.3 (left), 4.4 (middle) and 4.5 (right).

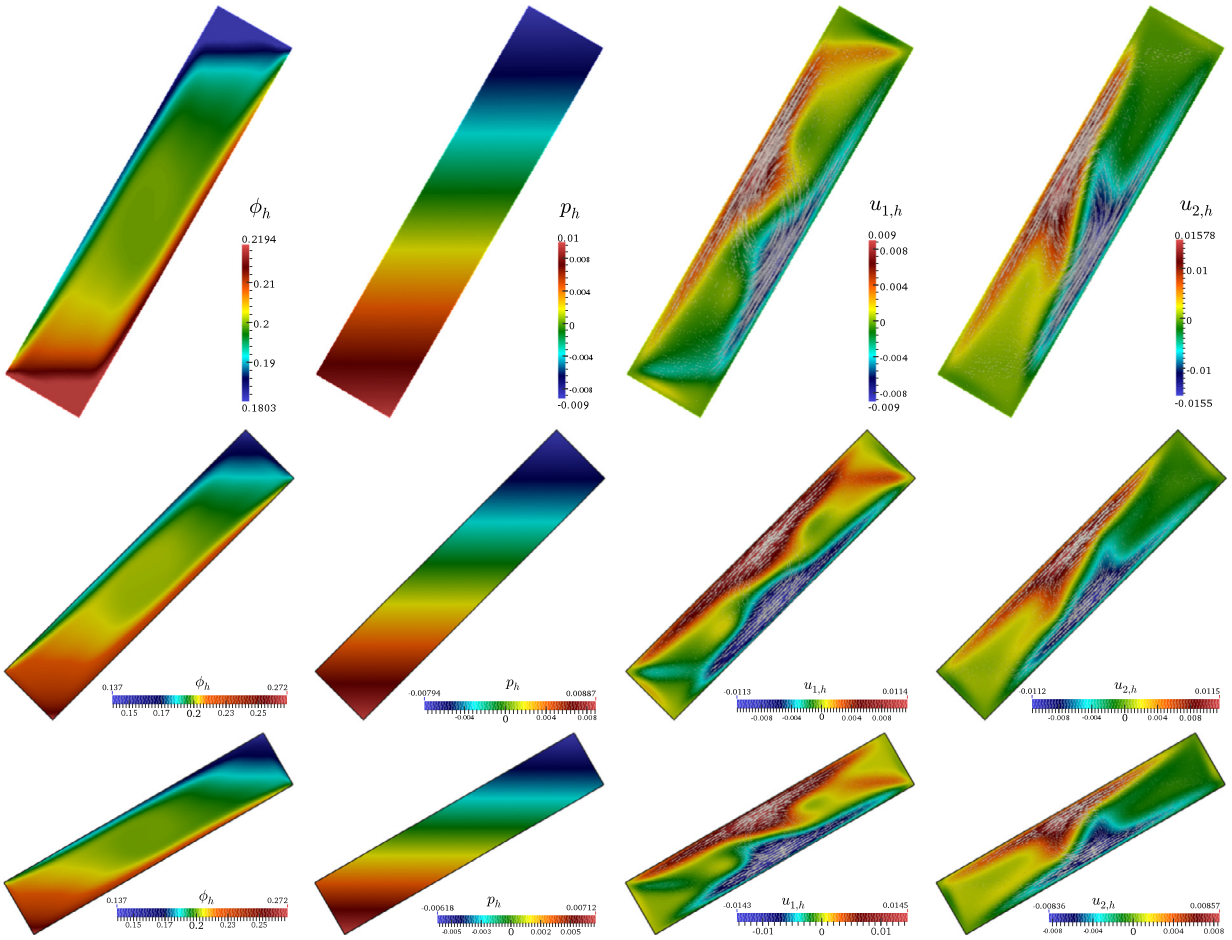


**Fig. 6.** Boycott effect in an inclined channel: FVE approximation of concentrations, pressure and velocities at $t = 500$ s for inclination angles of $\theta = \pi/3$ (top), $\theta = \pi/4$ (middle), and $\theta = \pi/6$ (bottom).

### *4.5. Sedimentation–consolidation in a tilted cylinder*

The FVE method is now tested in a 3D scenario by considering a cylindrical column of height 10 m and radius 1 m. The column is inclined so that it forms an angle of $\theta = \pi/3$ with the $y$-axis and a primal mesh of 22 235 vertexes and 126 261 tetrahedra is employed (Fig. 5, right). We use a timestep of $\Delta t = 0.01$ s, and we simulate the sedimentation process until $t = 200$ s. All physical parameters are taken as in the previous example and a snapshot of the approximate concentration, velocities and pressure is displayed in Fig. 8. Consistence with respect to the classical kinematic-wave theory of Kynch [26] is in general not expected, as discussed in e.g. [11]. However, for a non-inclined cylinder and if we set $A \equiv 0$ we recover the classical example of batch sedimentation, where we see that the horizontal interface is located at $z = 9.05201$ for $t = 150$ s, and at $z = 7.5812$ for $t = 375$ s. For this particular case we observe an agreement with the theoretical values predicted by the one-dimensional kinematic theory ($z = 9.04$ and $z = 7.6$, respectively, see also [13]).

## 5. Concluding remarks

We have presented a finite volume element formulation for the coupling of the incompressible Navier–Stokes equations and a parabolic equation describing the transport and consolidation of sediment in two and three spatial dimensions. The FVE formulation relies on a stabilized $\mathbb{P}_1$ finite element approximation of velocity, pressure and concentration fields. The method features satisfactory accuracy and stability that we have illustrated with some test cases, where optimal convergence orders are observed for space and time approximations.

Ongoing extensions of this work include the implementation of a fully implicit scheme with Newton linearization, a rigorous stability and convergence analysis of the proposed FVE method, the derivation of a mixed formulation for the coupled problem in terms of concentration, Cauchy stress and velocity; the development of residual-based a posteriori error indicators and mesh adaptivity that would permit us to accurately capture, for instance, the vorticity field (see e.g. [3]); and

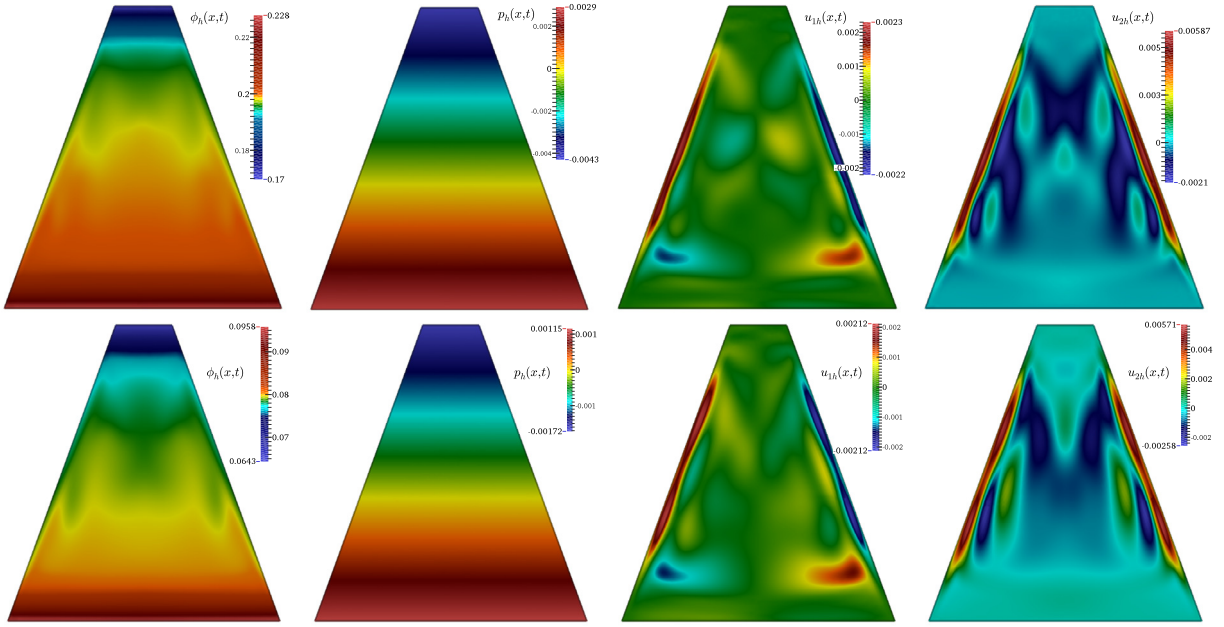


**Fig. 7.** Snapshot of the settling of a mixture in a vessel with downward-facing inclined walls, at $t = 100$ s for an initial concentration of $\phi_h(0) = 0.2$ (top) and $\phi_h(0) = 0.08$ (bottom).

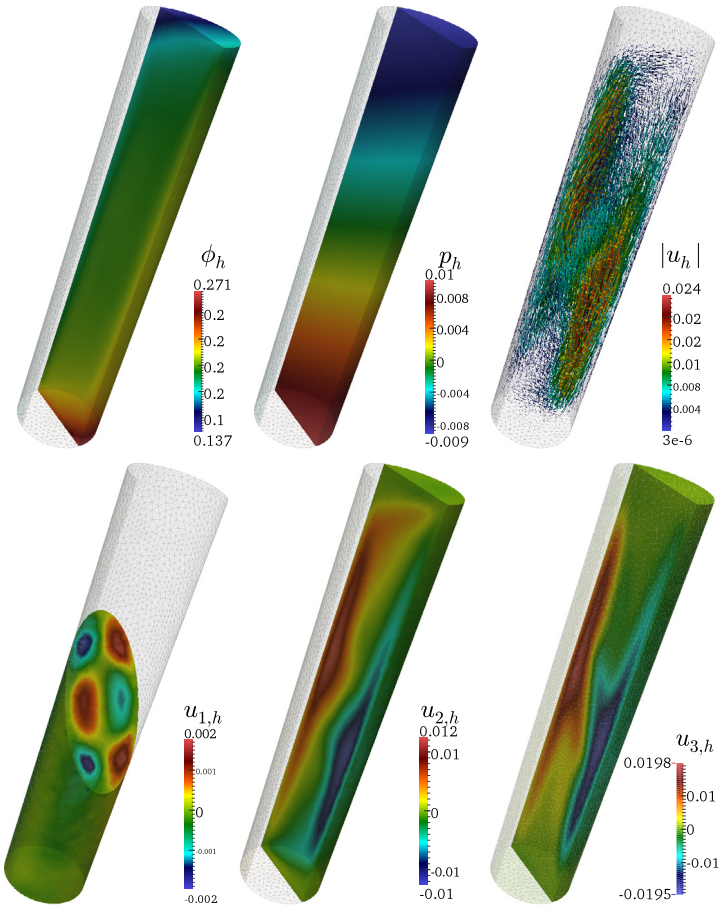


**Fig. 8.** Boycott effect in a cylinder: FVE approximation of concentrations, pressure and velocities at $t = 200$ s.

the construction of efficient solvers and preconditioning strategies that would allow substantial reductions in computational burden.

## Acknowledgements

The authors wish to thank Prof. Raimund Bürger and Prof. Kai Schneider for the stimulating discussions on the subject of this paper. In addition, RRB and HT acknowledge, respectively, the support by the University of Lausanne and by CONICYT-Chile through the FONDECYT project No. 11110264 and by the ANILLO project ACT 1118 (ANANUM).

## References

[1] A. Acrivos, E. Herbolzheimer, Enhanced sedimentation in settling tanks with inclined walls, J. Fluid Mech. 92 (3) (1979) 435–457.
[2] F. Ampofo, T.G. Karayiannis, Experimental benchmark data for turbulent natural convection in an air filled square cavity, Int. J. Heat Mass Transf. 46 (2003) 3551–3572.
[3] V. Anaya, D. Mora, R. Ruiz-Baier, An augmented mixed finite element method for the vorticity–velocity–pressure formulation of the Stokes equations, Comput. Methods Appl. Mech. Eng. 267 (2013) 261–274.
[4] B. Andreianov, K. Brenner, C. Cancès, Approximating the vanishing capillarity limit of two-phase flow in multi-dimensional heterogeneous porous medium, Z. Angew. Math. Mech. (2014), in press, http://dx.doi.org/10.1002/zamm.201200218.
[5] F. Auteri, N. Parolini, Numerical investigation of the first instabilities in the differentially heated 8:1 cavity, Int. J. Numer. Methods Fluids 40 (2002) 1121–1132.
[6] R.E. Bank, D.J. Rose, Some error estimates for the box method, SIAM J. Numer. Anal. 24 (1987) 777–787.
[7] Y. Bazilevs, V.M. Calo, J.A. Cottrell, T.J.R. Hughes, A. Reali, G. Scovazzi, Variational multiscale residual-based turbulence modeling for large eddy simulation of incompressible flows, Comput. Methods Appl. Mech. Eng. 197 (2007) 173–201.
[8] F. Betancourt, R. Bürger, R. Ruiz-Baier, H. Torres, C. Vega, On numerical methods for hyperbolic conservation laws and related equations modelling sedimentation of solid–liquid suspensions, in: G.-Q. Chen, H. Holden, K.H. Karlsen (Eds.), Hyperbolic Conservation Laws and Related Analysis with Applications, Springer-Verlag, Berlin, 2014, pp. 23–68.
[9] A.E. Boycott, Sedimentation of blood corpuscules, Nature 104 (1920) 532.
[10] C.-H. Bruneau, M. Saad, From steady to chaotic solutions in a differentially heated cavity of aspect ratio 8, Int. J. Numer. Methods Fluids 40 (2002) 1093–1107.
[11] R. Bürger, M. Kunik, A critical look at the kinematic-wave theory for sedimentation–consolidation processes in closed vessels, Math. Methods Appl. Sci. 24 (2001) 1257–1273.
[12] R. Bürger, C. Liu, W.L. Wendland, Existence and stability for mathematical models of sedimentation–consolidation processes in several space dimensions, J. Math. Anal. Appl. 264 (2001) 288–310.
[13] R. Bürger, R. Ruiz-Baier, K. Schneider, H. Torres, A multiresolution method for the simulation of sedimentation in inclined channels, Int. J. Numer. Anal. Model. 9 (2012) 479–504.
[14] R. Bürger, R. Ruiz-Baier, H. Torres, A stabilized finite volume element formulation for sedimentation–consolidation processes, SIAM J. Sci. Comput. 34 (2012) B265–B289.
[15] R. Bürger, W.L. Wendland, F. Concha, Model equations for gravitational sedimentation–consolidation processes, Z. Angew. Math. Mech. 80 (2000) 79–92.
[16] E. Burman, Interior penalty variational multiscale method for the incompressible Navier–Stokes equation: Monitoring artificial dissipation, Comput. Methods Appl. Mech. Eng. 196 (2007) 4045–4058.
[17] M.C. Bustos, F. Concha, R. Bürger, E.M. Tory, Sedimentation and Thickening, Kluwer Academic Publishers, Dordrecht, 1999.
[18] Z. Cai, On the finite volume element method, Numer. Math. 58 (1991) 713–735.
[19] C. Calgaro, E. Creusé, T. Goudon, A hybrid finite volume–finite element method for variable density incompressible flows, J. Comput. Phys. 227 (2008) 4671–4696.
[20] M.A. Christon, P.M. Gresho, S.B. Sutton, Computational predictability of natural convection flows in enclosures, Int. J. Numer. Methods Fluids 40 (2002) 953–980.
[21] R. Davis, A. Acrivos, Sedimentation of noncolloidal particles at low Reynolds numbers, Annu. Rev. Fluid Mech. 17 (1985) 91–118.
[22] S. Diehl, The solids-flux theory – confirmation and extension by using partial differential equations, Water Res. 42 (2008) 4976–4988.
[23] J.L. Guermond, P. Minev, J. Shen, An overview of projection methods for incompressible flows, Comput. Methods Appl. Mech. Eng. 195 (2006) 6011–6045.
[24] W.D. Hill, R.R. Rothfus, L. Kun, Boundary-enhanced sedimentation due to settling convection, Int. J. Multiph. Flow 3 (1977) 561–583.
[25] T.J.R. Hughes, G.R. Feijóo, L. Mazzei, J.-B. Quincy, The variational multiscale method – a paradigm for computational mechanics, Comput. Methods Appl. Mech. Eng. 166 (1998) 3–24.
[26] G.J. Kynch, A theory of sedimentation, Trans. Faraday Soc. 48 (1952) 166–176.
[27] M. Latsa, D. Assimacopoulos, A. Stamou, N. Markatos, Two-phase modeling of batch sedimentation, Appl. Math. Model. 23 (1999) 881–897.
[28] Z. Lin, R. Ruiz-Baier, C. Tian, Finite volume element approximation of an inhomogeneous Brusselator model with cross-diffusion, J. Comput. Phys. 256 (2014) 806–823.
[29] I. Lunati, P. Jenny, Multiscale finite-volume method for compressible multiphase flow in porous media, J. Comput. Phys. 216 (2006) 616–636.
[30] Z. Luo, H. Li, P. Sun, A fully discrete stabilized mixed finite volume element formulation for the non-stationary conduction–convection problem, J. Math. Anal. Appl. 404 (2013) 71–85.
[31] S.J. McCaffery, L. Elliott, D.B. Ingham, Two-dimensional enhanced sedimentation in inclined fracture channels, Math. Eng. Ind. 7 (1998) 97–125.
[32] S. McGee, P. Seshaiyer, Finite difference methods for coupled flow interaction transport models, Electron. J. Differ. Equ. 17 (2009) 171–184.
[33] A.S. Michaels, J.C. Bolger, Settling rates and sediment volumes of flocculated Kaolin suspensions, Ind. Eng. Chem. Fundam. 1 (1962) 24–33.
[34] L. Nadau, A. Sequeira, Numerical simulations of shear dependent viscoelastic flows with a combined finite element–finite volume method, Comput. Math. Appl. 53 (2007) 547–568.
[35] H. Nakamura, K. Kuroda, La cause de l'accélération de la vitesse de sedimentation des suspension dans les récipients inclinés, Keijo J. Med. 8 (1937) 256–296.
[36] E. Ponder, On sedimentation and rouleaux formation, Q. J. Exp. Physiol. 15 (1925) 235–252.
[37] I.S. Pop, F.A. Radu, M. Sepúlveda, O.P. Vera, Error estimates for the finite volume discretization for the porous medium equation, J. Comput. Appl. Math. 234 (2010) 2135–2142.
[38] A. Quarteroni, R. Ruiz-Baier, Analysis of a finite volume element method for the Stokes problem, Numer. Math. 118 (2011) 737–764.
[39] A. Quarteroni, R. Sacco, F. Saleri, Numerical Mathematics, 2nd ed., Texts Appl. Math., vol. 37, Springer-Verlag, Milan, 2007.

[40] F.A. Radu, I.S. Pop, P. Knabner, Error estimates for a mixed finite element discretization of some degenerate parabolic equations, Numer. Math. 109 (2008) 285–311.
[41] M. Sala, An object-oriented framework for the development of scalable parallel multilevel preconditioners, ACM Trans. Math. Softw. 32 (3) (2006) 396–416.
[42] U. Schaflinger, Experiments on sedimentation beneath downward-facing inclined walls, Int. J. Multiph. Flow 11 (1985) 189–199.
[43] U. Schaflinger, Influence of nonuniform particle size on settling beneath downward-facing inclined walls, Int. J. Multiph. Flow 11 (1985) 783–796.
[44] M. Tabata, D. Tagami, Error estimates of finite element methods for nonstationary thermal convection problems with temperature-dependent coefficients, Numer. Math. 100 (2005) 351–372.
[45] N.J. Walkington, J. Rulla, Optimal rates of convergence for degenerate parabolic problems in two dimensions, SIAM J. Numer. Anal. 33 (1996) 56–67.
[46] P. Wapperom, M.F. Webster, Simulation for viscoelastic flow by a finite volume/element method, Comput. Methods Appl. Mech. Eng. 180 (1999) 282–304.